



**HAL**  
open science

## A pulsatile developing flow in a bend

Marc Thiriet, J. Graham, R. Issa

► **To cite this version:**

Marc Thiriet, J. Graham, R. Issa. A pulsatile developing flow in a bend. *Journal de Physique III*, 1992, 2 (6), pp.995-1013. 10.1051/jp3:1992174 . jpa-00248799

**HAL Id: jpa-00248799**

**<https://hal.science/jpa-00248799>**

Submitted on 4 Feb 2008

**HAL** is a multi-disciplinary open access archive for the deposit and dissemination of scientific research documents, whether they are published or not. The documents may come from teaching and research institutions in France or abroad, or from public or private research centers.

L'archive ouverte pluridisciplinaire **HAL**, est destinée au dépôt et à la diffusion de documents scientifiques de niveau recherche, publiés ou non, émanant des établissements d'enseignement et de recherche français ou étrangers, des laboratoires publics ou privés.

## Classification

Physics Abstracts

02.60 — 47.60 — 87.45

**A pulsatile developing flow in a bend**

M. Thiriet, J.M.R. Graham and R.I. Issa

PFSU and Departement of Aeronautics, Imperial College and Royal School of Mines, London SW7 and LBHP, URA CNRS 343, Université Paris VII, 75251 Paris Cedex 05, France

(Received 3 April 1991, revised 13 February 1992, accepted 17 February 1992)

**Résumé .** — Un écoulement pulsé à basse fréquence d'un fluide incompressible visqueux a été étudié numériquement dans un coude, à  $90^\circ$ , de parois rigides et de section droite circulaire et constante, par la méthode des volumes finis. Les valeurs des paramètres adimensionnels gouvernant l'écoulement sont : un rapport d'amplitude de 1,25, un paramètre de Womersley de 4, un nombre de Reynolds crête de 358, un nombre de Dean crête de 113 ; le nombre de Strouhal varie entre 0,05 et 0,45. Aucune inversion du courant principal n'est observé et un unique vortex dans chaque demi-section droite apparaît. Les effets sur les tubes droits, l'un précédant et l'autre suivant le coude sont caractérisés par un décalage du pic de vitesse axiale vers le bord interne du tube en amont et la persistance de l'écoulement secondaire sur une longueur de plusieurs diamètres en aval. Les courants transversaux sont de très faible intensité quand la vitesse débitante de l'écoulement pulsé est beaucoup plus petite que la vitesse moyenne (composante stationnaire). Le cisaillement axial dont le maximum est situé sur le bord externe de la majeure partie du coude augmente en aval de la section d'entrée du coude puis reste constant sur une longueur d'environ 8 diamètres. Le maximum de la contrainte de cisaillement circonférentiel est localisé légèrement vers le côté externe du coude ; il est beaucoup plus faible que celui de la contrainte axiale (20 à 28 %). Les valeurs de ces contraintes augmentent pendant la phase accélératrice. La région à faible cisaillement est située au bord interne du coude sauf dans une courte zone d'entrée. Cependant, la présence d'un coude ne favorise le dépôt de particules solides circulantes que pendant la période de cycle à forte vitesse par rapport à une conduite rectiligne.

**Abstract .** — Low frequency pulsatile flow of an incompressible viscous fluid has been numerically investigated in a rigid  $90^\circ$  bend of circular cross-section, using the finite-volume method. The governing parameters are as follows : amplitude ratio of 1.25, Womersley parameter of 4, peak Reynolds number of 358, peak Dean number of 113, Strouhal number ranging from 0.05 to 0.45. With this set of input data, no flow reversal is observed and a single axial vortex occurs in the half cross-section. Upstream and downstream effects of the bend are mainly characterized by an inward shift of the peak axial velocity in the upstream straight tube and the persistency of the secondary motions several diameters down the exit straight pipe. Secondary motions, present in steady flow, weaken greatly when the unsteady axial component of the flow ( $W$ ) is lower than the mean flow  $\bar{W}$ . The axial shear stress  $\tau_a$ , whose maximum is more often located at the outer part of the bend, increases and remains nearly constant about 8 diameters downstream from the bend inlet. The circumferential shear stress  $\tau_c$  maximum, located slightly towards the outer bend, is 28% of  $\tau_a$  maximum, and 20% when  $W < \bar{W}$ . The magnitude of both  $\tau_a$  and

$\tau_c$  increases during the accelerative phase. The low shear region is more often located near the inner tube wall. However, the existence of bends in a tube network might increase the deposit of solid particles, with respect to straight pipes, only when  $W(t) > W$ , and locally at the inner edge.

### Nomenclature.

$a$	tube radius
$d$	tube diameter
$De$	Dean number
$k$	curvature ratio
$L$	local length
$R$	radius of curvature
$Re$	Reynolds number
$St$	Strouhal number
$T$	period
$u$	circumferential velocity
$v$	radial velocity
$w$	axial velocity
$x$	circumferential angular coordinate
$y$	radial coordinate
$z$	axial (angular in bend) coordinate
$\alpha$	Womersley parameter
$\gamma$	amplitude ratio
$\nu$	kinematic viscosity
$\tau$	shear stress
$\omega$	angular frequency

### Subscripts :

a	axial
c	circumferential
m	amplitude of sine wave
p	peak value
s	steady component
2	secondary flow

### 1. Introduction.

The permeability of the arterial wall and the development of the atherosclerotic plaque is influenced by the wall shear. The circulatory bed is characterized by numerous sites of curvature, branching and bifurcations, and by cross-sections of varying dimensions along the network. In addition, a huge variability in geometry of the vessel network exists between the human subjects. The arterial wall is viscoelastic ; the mechanics of the blood flow is thus coupled to the mechanics of the compliant wall. Furthermore, the wall is subjected to a highly variable biochemical environment which induces mechanical and geometrical changes. Last but not least, the blood, which behaves like a non-newtonian fluid, is conveyed by a periodic non-zero

mean pressure gradient. Consequently, approximations are currently made in order to model blood flow in the vascular tree, so much more it exists a huge between-subject variability. The first unavoidable stage of a three-dimensional unsteady flow study is focused on bend flow.

Purely oscillatory flow in a fully-developed regime was investigated initially. In this case, an axial two-vortex system appears in the half cross section for large values of the Reynolds number of the secondary flow or small values associated with high values of the unsteadiness parameter  $\alpha$  (Lyne 1970, Bertelsen 1975). However, the superimposition of an oscillatory flow on a steady component is more relevant to cardiovascular problems. A finite-difference solution of a laminar, pulsatile (with unit ratio of amplitude to mean of the velocity waveform  $\gamma$ ), fully-developed flow in a curved pipe was done by Rabadi *et al.* (1980), using a  $21 \times 21$  mesh in the half cross-section. This was done mainly for a Dean number  $De = 100$  and a curvature ratio  $k = 1/100$  ( $k = a/R$  :  $a$  : tube radius,  $R$  : radius of curvature of the pipe axis). With increasing  $\alpha$  ( $1 \leq \alpha \leq 15$ ), the magnitude of the wall shear decreases as well as its variation within the period. Furthermore a considerable variation of the secondary flow intensity during one cycle was observed for low values of  $\alpha$ . Laser-Doppler measurements of the axial velocity and of the secondary velocity along selected vertical traverse lines were carried out by Talbot and Gong (1983), in a  $180^\circ$  bend. In their experiment II (for  $\gamma = 1.02$ ,  $k = 1/7$ ,  $\alpha = 12$ , and  $De = 372$ ), reverse axial flow occurred at the inner bend during the decelerating phase. As the deceleration proceeded, an embedded vortex was found to be associated with the outer and upper borders of a "jet-like" secondary motion. Moreover, the secondary velocity profiles suggest the existence of an additional vortex in the inner half of the cross section, near the centerplane, at  $30^\circ$  from the bend entry. During the accelerative phase, the axial flow reversal disappeared, whereas the secondary motion kept its complex features. The pressure-gradient waveforms of Talbot and Gong (1983) were used by Chang and Tarbell (1985) for their numerical simulations of fully-developed pulsatile flow. A uniformly spaced non-staggered  $21 \times 21$  grid was employed in the half cross-section of the curved tube. At the beginning of the flow deceleration, the secondary flow was characterized by a single vortex with an inner center and complex paths in the outer half of the cross section. At the mid-time of flow deceleration, an embedded vortex appeared near the inner wall. A weak outer vortex, whose current was opposite to that of the others, was also observed near the plane of curvature. This secondary flow disappeared as early as about the last third of the duration of the decelerating phase. Twin embedded vortices occurred at the end of flow acceleration. Very recently, Hamakiotes and Berger (1988) studied the effect of  $De$  ( $0.76 \leq De \leq 756$ ) on fully developed pulsatile flow, with  $k = 1/7$ , for  $\alpha = 15$  and  $\gamma = 1$ . They used a staggered non-uniform  $14 \times 19$  mesh within the half cross-section. The secondary flow became much more complex and an inward cross-motion of fluid along the center plane was obtained for  $De$  approximately greater than 227 ( $Re \sim 600$ ).

In summary, unsteady flow is much more complicated with flow reversal and embedded cross-vortices as within larger fluid movements. The characteristics of these flow properties have been shown to depend on the values of the governing parameters for fully-developed flow. The present work is aimed at carrying out a numerical study of the development of a low frequency pulsatile laminar flow in a  $90^\circ$  bend of uniform circular cross-section ( $k = 1/10$ ). The Womersley parameter equals 4, this value corresponding to the condition in the human femoral artery.

## 2. Method.

**2.1 GOVERNING EQUATIONS.** — The pulsatile flow of an incompressible, viscous, newtonian fluid in a rigid curved tube of uniform circular cross-section, is studied theoretically using a toroidal coordinate system  $(x, y', z)$ . Within the cross section, the polar coordinates  $x, y'$  define respectively the angle between the position vector and the centerplane and the distance from the center of the cross section. The axial coordinate  $z$  measures the angle between the cross section of interest and the bend inlet. The following normalized variables can be introduced :

$$y = y'/a, \quad s = -Rz/a, \quad D = (R + y' \cos x)/R, \quad u, v = (W_p^2/R\omega)^{-1}u', v'; \\ w = W_p^{-1}w',$$

where  $\omega$  is the angular frequency of oscillation and  $W_p$  the cross-sectional mean of the peak axial velocity (prime denoting dimensional quantity). In unsteady flow, when the temporal inertia forces of the secondary flow are mainly balanced by the radial pressure gradient, a scale for the secondary velocity is given by  $U_2^* \sim W^{*2}/\omega R$ , where  $W^*$  is a characteristic axial velocity (here taken as  $W_p$ ). The dimensionless governing equations (mass and momentum conservation) become :

$$(1/y + k \cos x/D)u + u_y - (k \sin x/D)v + (1/y)v_x + (St_p/D)w_s = 0 \quad (1)$$

$$u_t + St^{-1}(uu_y + (v/y)(u_x - v) + (St_p/D)w(u_s - St_p k \cos xw)) \\ = -p_y + \alpha^{-2}((1/D)\partial/\partial s(u_s - k St_p \cos xw - D St_p w_y) \\ - (1/yD)\partial/\partial x(D(v_y - v/y - (1/y)u_x))) \quad (2.1)$$

$$v_t + St^{-1}(uv_y + (v/y)(u + v_x) + (St_p/D)w(k St_p \sin xw + v_s)) \\ = - (1/y)p_x + (\alpha^{-2}/D)(\partial/\partial y(D(v_y + v/y - (1/y)u_x)) \\ + \partial/\partial s((1/D)(v_s + k St_p \sin xw) - (St_p/y)w_x)) \quad (2.2)$$

$$w_t + St^{-1}(uw_y + (v/y)w_x + (w/D)(St_p w_s + k(u \cos x - v \sin x)) \\ = (1/St_p D)p_s + (\alpha^{-2}/y)\partial/\partial y(y(w_y + (k \cos x/D)w - (1/D)St_p u_s) \\ + \partial/\partial x((1/y)w_x - (1/D)((1/St_p)v_s + k \sin xw)) \quad (2.3)$$

where subscripts  $x, y, s$  ( $s = Rz$ ) denote partial derivatives,  $St = (\omega^2 a R / W_p^2)$  and  $St_p = R\omega / W_p$ .

Several non-dimensional quantities appear in these equations. The Womersley parameter  $\alpha = a(\omega/\nu)^{1/2}$  ( $\nu$  : kinetic viscosity) may be defined as the ratio of inertial forces associated with the local acceleration to the viscous forces per unit mass. The ratio  $\alpha^2/Re$  defines a frequency parameter, the Strouhal number  $St$ , which determines the time available for vortex formation. It gives also the ratio of the local acceleration to the convective acceleration.  $St$  corresponds in the above equations to the Strouhal number for secondary flow, the corresponding Reynolds number being :  $Re_2 = W_p^2 k / \omega \nu$ .  $St_p$  is the Strouhal number calculated from the peak Reynolds number  $Re_p = W_p a / \nu$ . As for the steady case, laminar bend flows are also characterized by the Dean number,  $De = k^{1/2} Re$ , which is proportional to the square root of the product of the inertial and centrifugal forces to viscous forces. This work has been carried out with a single velocity waveform. The effect of the amplitude ratio  $\gamma$  has thus not been studied. Flow conditions in curved tubes are also defined by the following similarity parameter  $W_p T / d$  ( $T$  : period), used to specify the degree of disturbances in oscillatory flow.

**2.2 COMPUTATIONAL MODEL.** — A finite-difference scheme is used to solve the developing quasi-steady laminar flow of incompressible fluid through a  $90^\circ$  bend. The curved section of tube is interposed between 2 straight sections, a short (length of  $3.6 d$ ) upstream and a longer one (length of  $8.1 d$ ) downstream. Briefly, the finite-volume method employs a hybrid of up-wind and central differencing procedure proposed by Caretto *et al.* (1972). The solution of the set of discretised equations is achieved by the Piso algorithm developed by Issa (1982). The sequence of main operations of the solution procedure is as follows : (i) the pressure field is guessed, (ii) the predictor-step momentum equations are solved to get a first approximation of the 3 components of the velocity field, (iii) the first corrector step pressure-increment equation is solved to obtain a new pressure field, which gives a corrected velocity field satisfying the continuity equation, (iv) the second corrector step pressure-increment equation with new pressures calculates new velocities. The residuals for each equation solved over the entire field must have decayed systematically below a specified threshold to obtain a convergence. Otherwise, a new iteration with the same steps is initiated. The velocity field in the 3 directions is computed using a line-by-line counterpart of Gauss-Seidel iteration employing the tri-diagonal matrix scheme. The pressure field is calculated by the Stone implicit method (Stone, 1968). The number of line iterations at each complete sweep through the domain varies for each variable ; eight iterations are used for the 3 components of the velocity and 250 for the pressure. Besides, the velocities were under-relaxed (under-relaxation factor of 0.5).

The velocity nodes are staggered with respect to the storage locations of all other variables. The domain is discretised into a finite number of hexahedra. The pressure is stored at the center of the cell while the three components of the velocity  $u$  (circumferential direction  $x$ ),  $v$  (radial direction  $y$ ), and  $w$  (axial direction  $z$ ), are defined at the center of the faces of the hexahedron for which these velocities are normal. Figure 1 shows the grid system. The axial length of the cell  $dz$  was smaller in the curved tube and in the adjoining straight sections;  $dz$  was equal to  $5 dx$  and increased regularly to  $10 dx$  toward the inlet of the upstream straight pipe and the outlet of the downstream straight tube. A coarse mesh ( $7 \times 7 \times 48$ ) was used because of the limit in available memory size, the computation being done on a Control Data computer CY 855, under NOS operating system.

The inlet conditions correspond to the Womersley solution (Womersley, 1955) applied to a sinusoidal pressure gradient (amplitude of 2.66 kPa, mean of 13.33 kPa, cycle period  $T$  of 1 s) in a straight rigid tube. The resulting velocities were superimposed on a steady Poiseuille flow. The temporal variations of the cross-sectional average of the axial velocity is displayed also in Figure 2 ( $\gamma = 0.8$ ). The values of the governing parameters are as follows :  $\alpha = 4$ ,  $Re = 199$ ,  $Re_p = 358$ ,  $Re_2 = W_p^2 k / \omega \nu = 181$ . The mean Dean number  $De = 63$ , while  $De_p = 113$ . In our test, with the amplitude of the oscillatory component lower than the steady component,  $St(t)$  remains lower than 0.5 throughout the pulse cycle. The numerical test was treated as quasi-steady, since the local acceleration terms ( $\partial \mathbf{u} / \partial t$ ) were considered negligible with respect to the other convective terms (inertial forces linked to the convective acceleration  $\mathbf{u} \partial \mathbf{u} / \partial \mathbf{x}$  and the centrifugal forces, see left-hand side of equations 2.1 - 2.3). The developing bend flow was computed for several axial velocity profiles at the entrance of the upstream straight pipe, corresponding to the normalized times: 0 (beginning of the second half stage of flow acceleration), 0.13, 0.26 (beginning of the decelerating phase), 0.39, 0.52, 0.61, 0.74 (beginning of the accelerating phase), 0.87, 1.

**2.3 EXPERIMENTS.** — The perspex bend, of  $25.5 \pm 0.2$  mm internal diameter ( $d$ ) was located  $57 d$  downstream from a constant head reservoir, connected to a straight tube by a converging nozzle. The straight tube downstream from the test section had a length of  $43 d$ . The plane of measurement, 1.5 mm above the plane of curvature, was slightly oblique due to the refraction

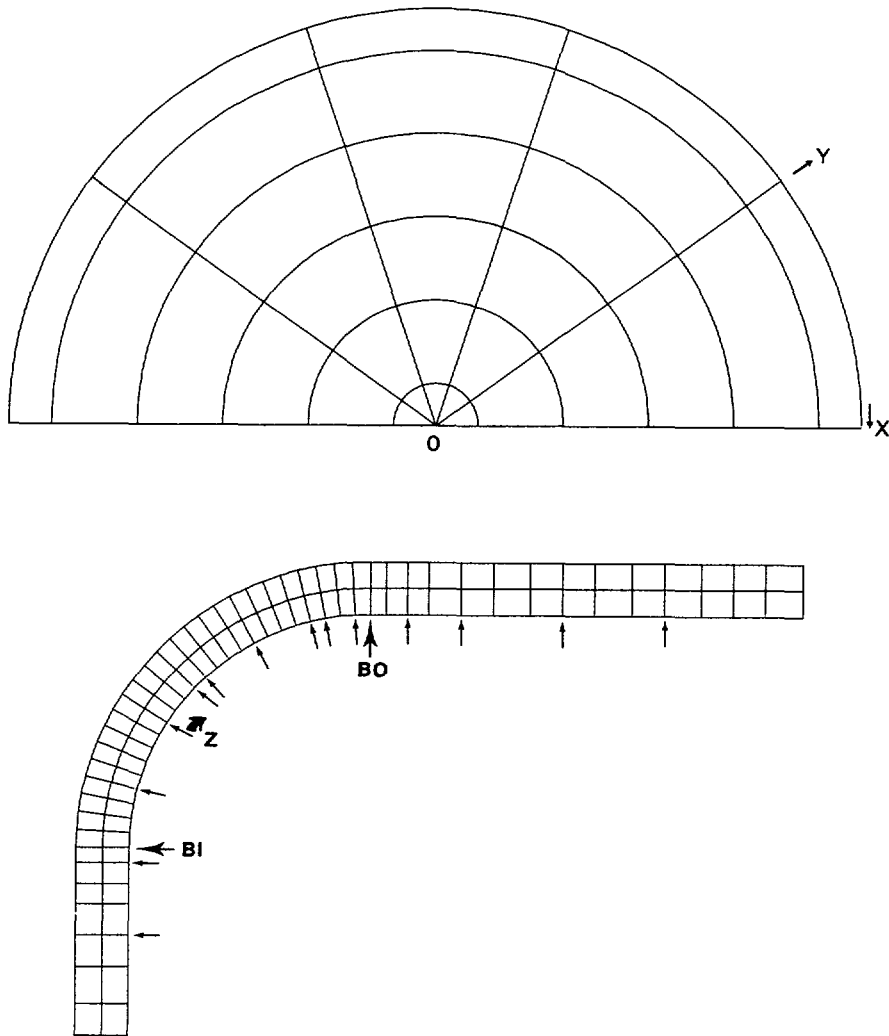


Fig. 1. — Grid system in the cross section (top) and along the pipe (bottom).  $X$  is the circumferential —,  $y = y'/a$  the radial — and  $z$  the axial coordinate ; the arrows indicate the location of selected cells used to display the results (the shear stress values, at the cell center, are interpolated).

of the laser beam at the pipe inner wall ( $\sim 0.8^\circ$  from the horizontal). The bend was machined from 2 plexiglass plates, fitted in the plane of symmetry. The assembled curved tube had flat polished outer faces of width 70 mm and of height 38.10 mm. The test section was supported horizontally on an aluminium beam. Water was conveyed by gravity from the constant head reservoir ; the flow speed was set by a rotameter. After travelling down the tubes, the water passed into a large sump tank from where it was pumped back to the head reservoir.

Velocity components were measured with a laser-doppler velocimeter, operating in dual beam forward scattering mode. This comprised a 5 mW helium-neon laser (Spectra Physics 120) of wavelength 632.8 mm, a 50 mm beam splitter (TSI 915), a Bragg cell for acoustico-optical frequency shifting (TSI 980), transmitting- receiving and collecting lenses of respectively

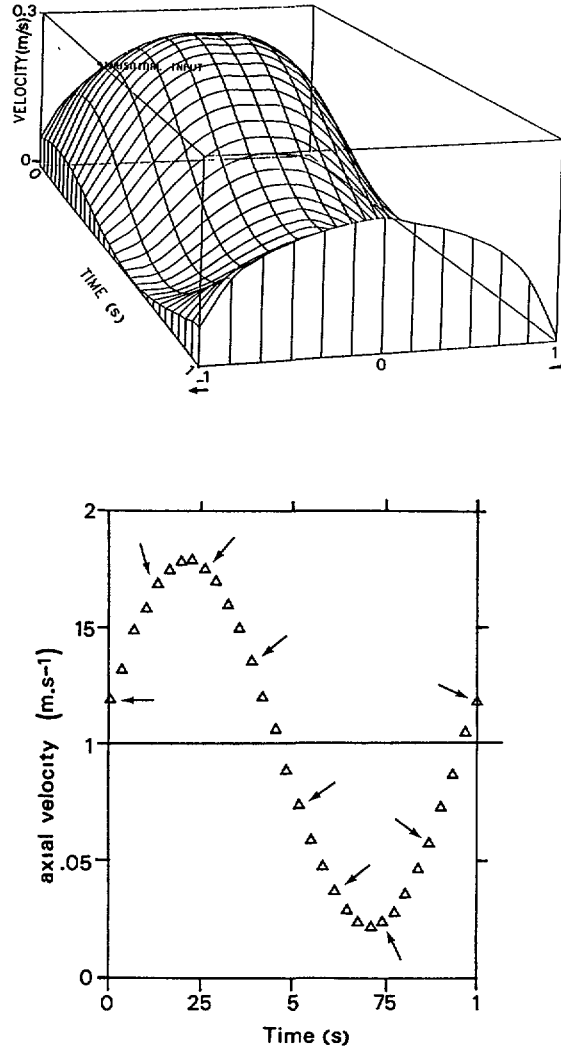


Fig. 2. — Top : temporal variations of the cross-sectional average of the axial velocity during the oscillatory cycle (amplitude of  $0.08 \text{ m.s}^{-1}$ , mean of  $0.1 \text{ m.s}^{-1}$ ). The arrows indicate the time at which the results are plotted. Bottom : axial velocity profiles throughout the oscillatory period calculated from the Womersley solution applied to a sinusoidal pressure gradient ( $10.7\text{-}16 \text{ kPa}$ , frequency of  $1 \text{ Hz}$ ) with a superimposed Poiseuille flow. The profiles are displayed each  $1/31$  of the period. The axial velocity at the left wall are not given in the present (3-D) plotting box.  $y = -1$  correspond to the inner wall, while  $y = 1$  is the outer wall.

247.3, 246 and  $200 \text{ mm}$  focal length, and finally a photomultiplier of aperture size  $256 \text{ }\mu\text{m}$ . The photo-detector signal was demodulated with a frequency tracker (TSI 1090). The tracker operated at an average tracking rate of 0.5. The measuring volume had a diameter of  $\sim 91 \text{ }\mu\text{m}$ , a length of  $\sim 0.92 \text{ mm}$  and a height of  $\sim 0.90 \text{ }\mu\text{m}$ ; the number of fringes was about 28. Both measurement sites and axial velocities were corrected for refraction. The inlet flow was checked to be a Poiseuille motion and measurements were performed at  $z = 15^\circ, 45^\circ$  and  $75^\circ$ .

However an error on the actual location of the measurement point of 2% has been estimated. The velocity was measured at a given point several times (to obtain a temporal mean and check the variability) and at different periods (to test the reproducibility). The noise and the flow fluctuations are responsible for an error of 3% on the velocity.

### 3. Results.

In figure 3, experimental profiles of the axial steady flow velocity are compared to the numerical values, extrapolated for the plane of measurement, at stations  $15^\circ$  ( $1.3 d$ ),  $45^\circ$  ( $3.9 d$ ),  $75^\circ$  ( $6.5 d$ ) and  $+ 2 d$ . A second, but lower, maximum is observed between the mid-vertical plane and the inner bend. A qualitative agreement is obtained between the two sets of data. The wall shear appears to be overestimated in the numerical model, which uses a coarse grid in the cross-section, especially at the inner wall.

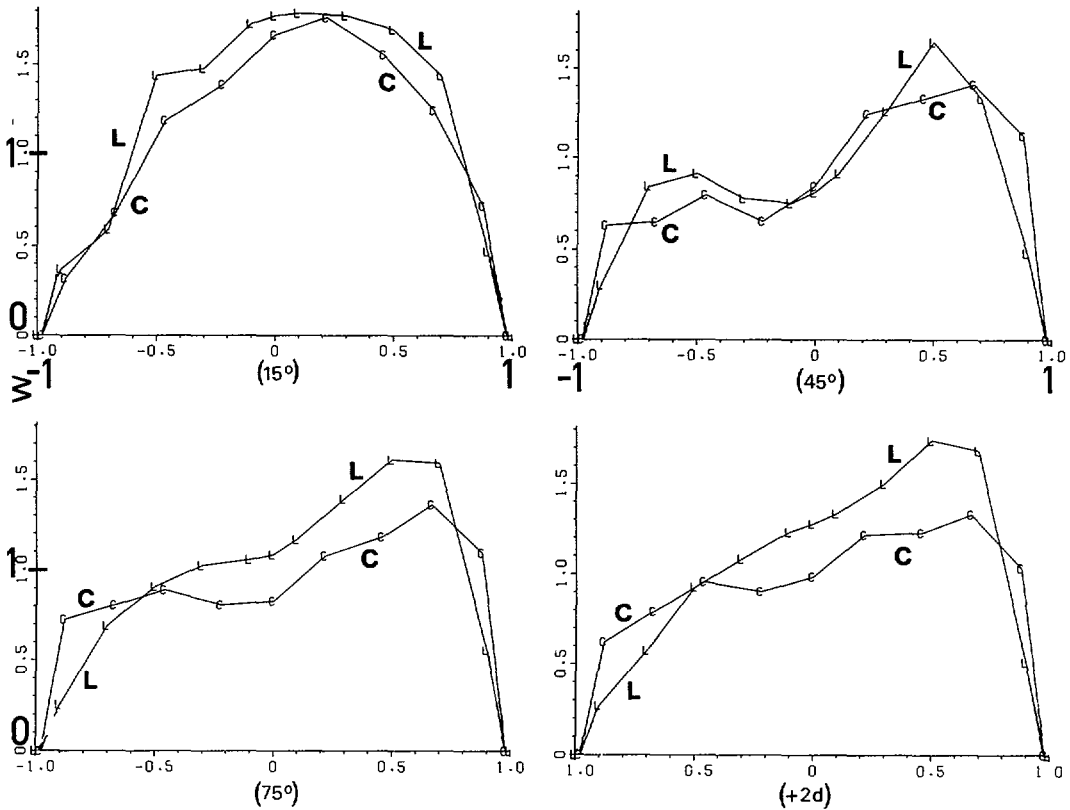


Fig. 3. — Comparison between the measured axial velocities ( $L$ ) in a  $90^\circ$  bend for  $De = 433$  and the numerical extrapolated values ( $C$ ), in a plane located at  $0.1 a$  from the centerplane, at  $15^\circ$  (upper left panel), at  $45^\circ$  (upper right panel), at  $75^\circ$  (lower left panel), and at  $2 d$  in the downstream straight pipe (lower right panel). Steady flow ( $Re = 1370$ ,  $De = (a/R)^{1/2} Re = 433$ ).

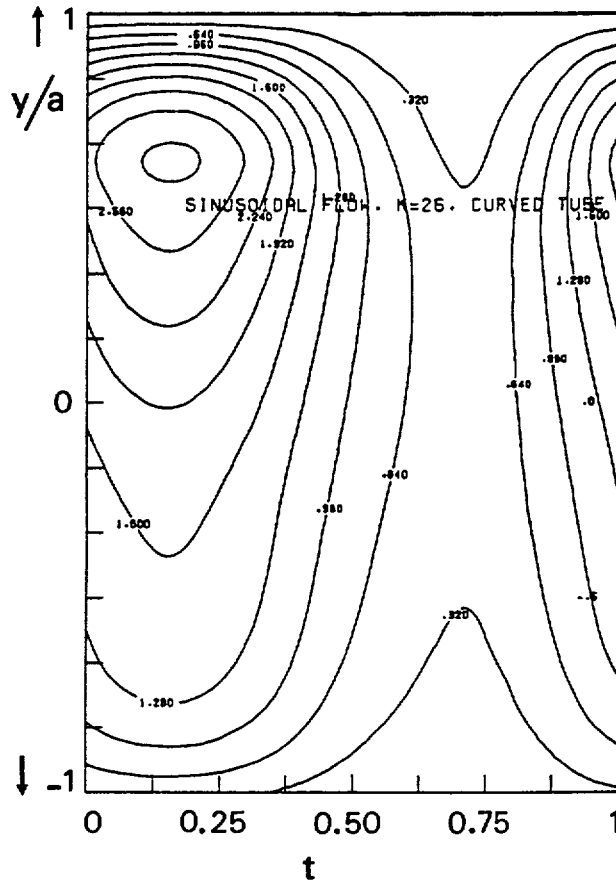


Fig. 4. — Axial isovelocity contours in the centerplane computed at  $61.2^\circ$  from the bend entry throughout the pulse cycle. The outer wall corresponds to the upper horizontal axis ( $y = 1$ ).

An example of axial isovelocity contours in the centerplane for a fixed cross section of the curved tube is depicted in figure 4. For high values of the pulsatile flow, the "isovels" reveal an outer shift of the peak axial velocity, here at  $z = 61.2^\circ$ . For low values of the pulsatile flow, the profile seems to be more symmetrical. This feature is confirmed by the axial isovelocity contours in the centerplane of the test section plotted in figure 5 at different times. The distortion of the axial velocity profiles in the curved tube becomes slight at  $t = 0.61$  (end of flow deceleration) and even more at  $t = 0.74$  (beginning of flow deceleration,  $W$  being lower than at  $t = 0.61$ ). Figure 6 shows the axial isovelocity contours in the half cross-section at selected sites along the test segment. The isovel shape, as in the case of contours obtained for bend flow with a Poiseuille entrance, is distorted by the strong secondary motion. The region of high axial velocity, displaced towards the outside bend is expanding in the circumferential direction. However, this expansion is smaller than for the case of Poiseuille entrance flow for which the contours are crescent shaped. At the beginning of the accelerating phase, the flow is almost symmetrical, although a slight outer shift of the peak velocity is observed, at least, for  $z \geq 32.4^\circ$ . Moreover, the peak velocity occurs in the region of the centerplane. The vector plots of the secondary flow show the difference in magnitude of the secondary velocity

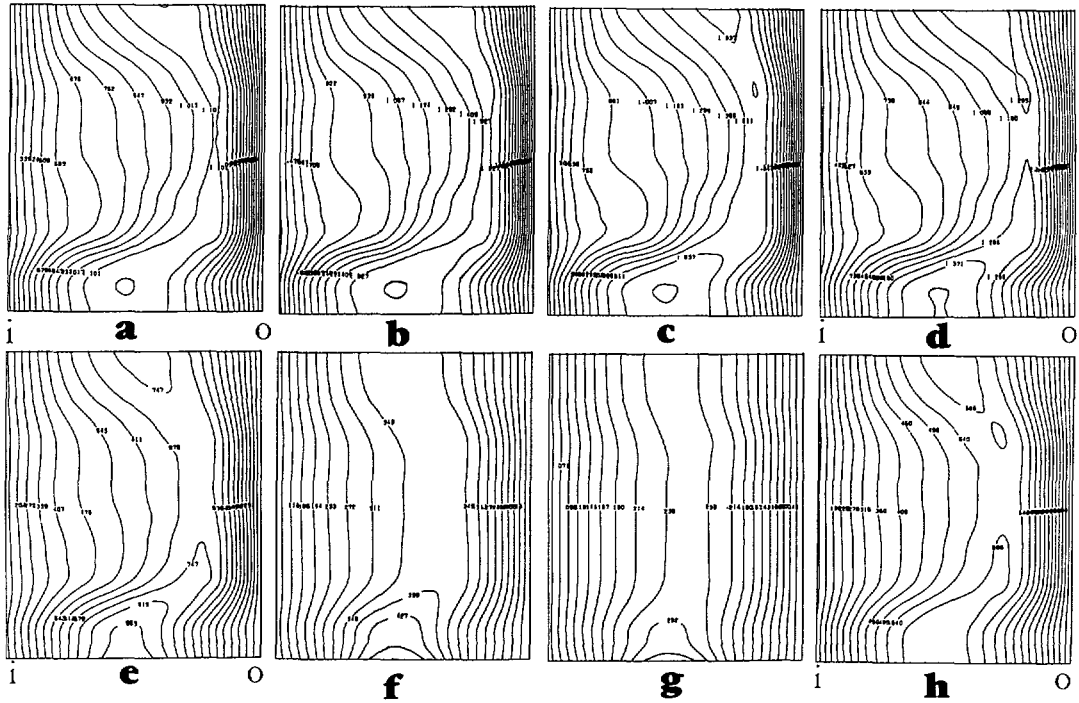


Fig. 5. — Axial isovelocity contours in the centerplane computed at different times during the pulse cycle (from a to h :  $t/T = 0, 0.13, 0.26, 0.39, 0.52, 0.61, 0.74$  and  $0.87$ ) from the selected cross sections (from the inlet, at the bottom of each figure, to the outlet section :  $-1.7d, -0.4d, 0^\circ, 14.4^\circ, 32.4^\circ, 43.2^\circ, 46.8^\circ, 61.2^\circ, 75.6^\circ, 79.2^\circ, 86.4^\circ; +0.7d, +1.7d, +3.6d, +5.5d$  and  $+7.4d$ ). The inner wall is located at the left side (1) and the outside bend at the right side (0).

between the beginning of flow deceleration (i) and the beginning of flow acceleration (ii), more especially as the scaling factor is three times greater in (ii) than in (i) (Fig.7). The cross flow is negligible when the magnitude of axial flow is near zero. In this studied case of pulsatile flow, the secondary motion, at  $\sim 34^\circ$  from the bend inlet, is  $\sim 20\%$  of the axial component at the beginning of flow deceleration and  $\sim 10\%$  of the axial component when  $W$  is in the range of its lowest values. Throughout the pulse cycle, along the entire curved tube, only one-vortex system in the half cross-section is observed. The vortex center is located nearer to the vertical diameter and to the centerplane than for Poiseuille entrance flow.

Another variable, very important from, at least, a physiological point of view, is the shear stress. In particular it plays a role in particle deposition on the vessel wall, as the atherosclerotic plaques tend indeed to form preferentially in low shear regions (Caro *et al.*, 1969). Furthermore, the flow pattern has been indeed shown to influence the cell dispersal over the cross section (Snabre *et al.*, 1987). The non-uniform adhesion of monocytes to the endothelial layer of the arterial wall might be explained by the distribution of the wall shear, the transverse migration depending on the state of aggregation of the flowing suspension of red blood cells (Mills and Snabre, 1987). The variations of the numerically predicted axial ( $\tau_a$ ) and circumferential ( $\tau_c$ ) shear stresses are plotted against the axial distance  $z$ , at constant circumferential coordinate, and against the circumferential angle  $x$ , in selected sections along the pipe model, respectively, in figure 8, for 2 different times of the sinusoidal cycle. At both times,  $\tau_a$  is higher

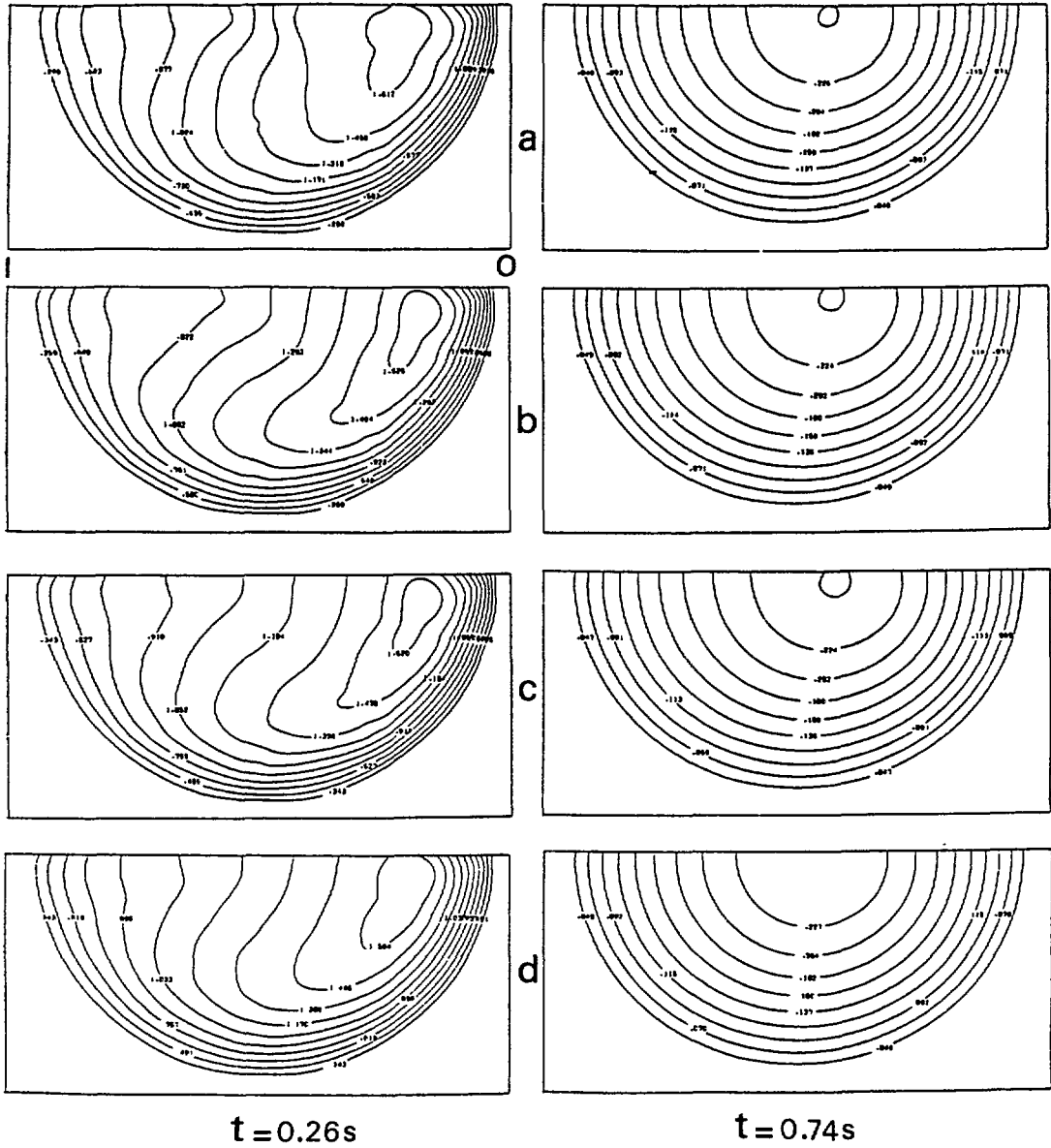


Fig. 6. — Axial isovelocity contours in the half cross section. From top to bottom, the figures correspond to selected sections selected sections located at 32.4° (a), 61.2° (b), 86.4° (c) and +1.7d (d). The isovels are displayed at the beginning of flow deceleration (left,  $t = 0.26$ ) and at the beginning of flow acceleration (right,  $t = 0.74$ ). I : inner wall, O : outer wall.

near the inner wall in the entrance region of the curved tube and in the adjoining segment of the upstream straight pipe, as in steady flow .

It becomes higher near the outer wall, 1.5  $d$  downstream from the bend inlet. But, its value decreases a lot between the beginning of flow deceleration and the beginning of flow acceleration ; the magnitude of the fall reaches 90% in the bend entrance and slightly more in

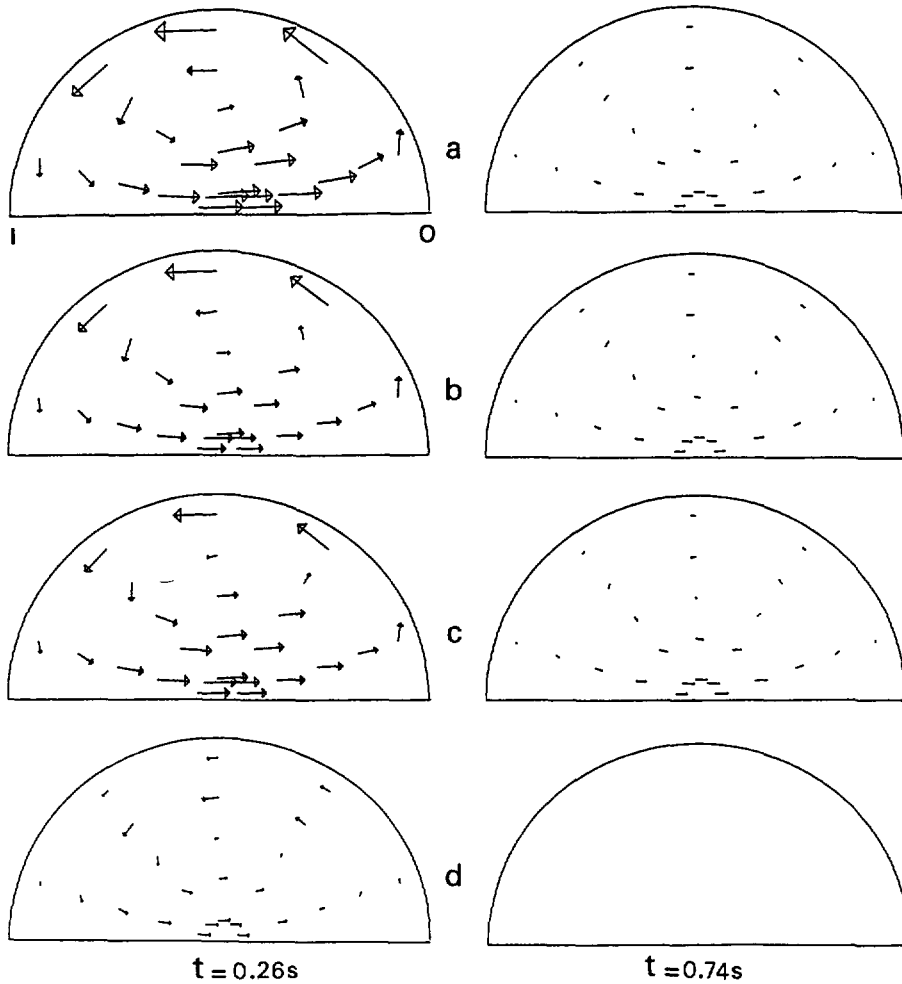


Fig. 7. — Vector plots of secondary flow in the half cross-section in selected cross sections (from top to bottom, a :  $34.2^\circ$ , b :  $63^\circ$ , c :  $88.2^\circ$ , d :  $+2d$ ) at the beginning of flow deceleration (left) and at the beginning of flow acceleration (right). I : inner wall, O : outer wall.

the exit region. The value of  $\tau_a$  appears to be much more uniform in the cross-section when the unsteady axial component of the flow becomes lower than the mean flow. The maximum of  $\tau_c$  is located near the upper (lower) wall, slightly towards the outer wall. There is an inner shift of the peak at the bend entry. The magnitude of the maximum of  $\tau_c$  is about 3.5 times lower than peak  $\tau_a$  near peak flow, and the difference becomes greater near minimal flow. The maximum of  $\tau_c$  increases up to  $34^\circ$ , at both times, from the bend entry and decreases further downstream, and then becomes zero at the outlet of the downstream straight pipe with the disappearance of the secondary motion. The temporal variations in  $\tau_a$ , for a given circumferential coordinate  $x$ , along the test section, are presented in figure 9. As suggested by the axial velocity changes throughout the cycle, the magnitude of  $\tau_a$  decreases during the deceleration phase. Figure 9 confirms the much smaller spatial variations in  $\tau_a$  during the low flow stage, whatever  $x$ , and the rapid shift within the bend of the location of peak  $\tau_a$  from the inside to the outside wall. A

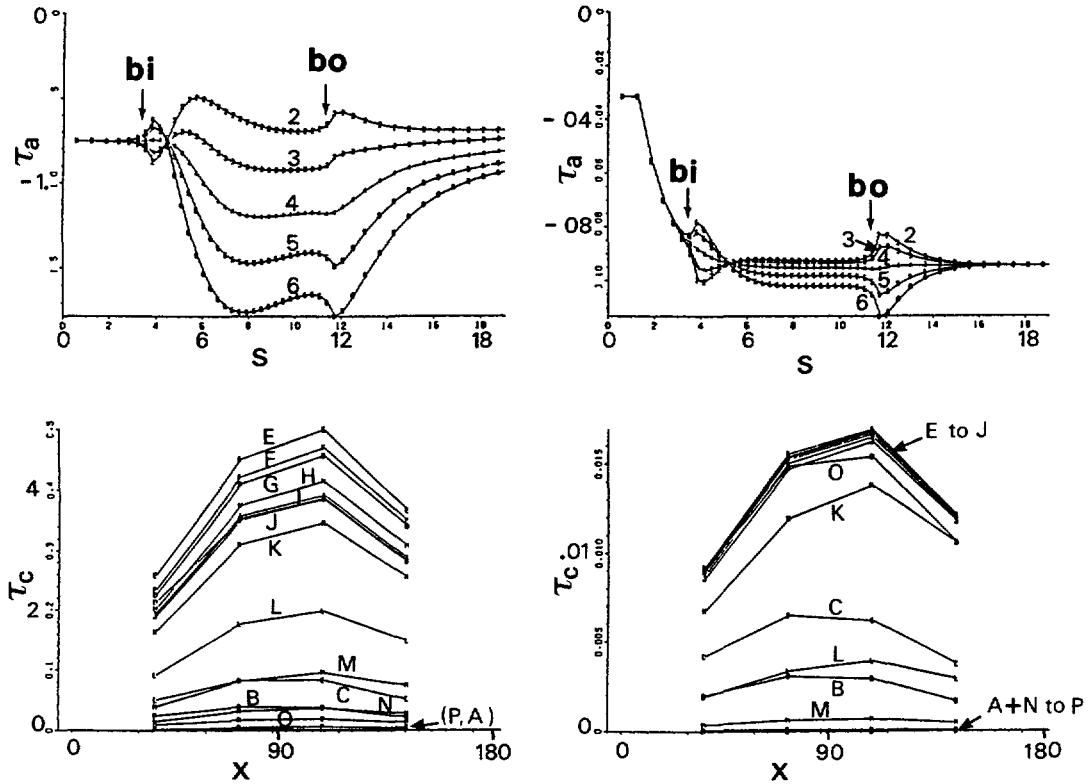


Fig. 8. — Top : axial shear stresses  $\tau_a$  (in  $N.m^{-2}$ ) against longitudinal distance along the test section ( $s = L/d$  in the straight tubes,  $s = Rz/d$  in the curved tube) for different circumferential angle  $x$  (2 :  $18^\circ$  ; 3 :  $54^\circ$  ; 4 :  $90^\circ$  ; 5 :  $126^\circ$  ; 6 :  $162^\circ$ ) at the beginning of flow deceleration (left) and at the beginning of flow acceleration (right). bi : bend inlet ; bo : bend outlet.  
 Bottom : circumferential shear stresses  $\tau_c$  (in  $N.m^{-2}$ ) against circumferential angle  $x$  in different sections of the duct. (A :  $-1.4d$  ; B :  $-0.2d$  ; C :  $1.8^\circ$  ; D :  $16.2^\circ$  ; E :  $34.2^\circ$  ; F :  $45^\circ$  ; G :  $48.6^\circ$  ; H :  $63^\circ$  ; I :  $77.4^\circ$  ; J :  $81^\circ$  ; K :  $88.2^\circ$  ; L =  $+0.9d$  ; M :  $+2.0d$  ; N :  $+3.9d$  ; O :  $+5.8d$  ; P :  $+7.8d$ ) at the same times of the cycle as the top figures.

larger magnitude change during the cycle is observed near the outer bend than near the inner edge. The temporal variations in  $\tau_c$ , at 2 selected cross sections (mid-part and exit region of the curved tube), are given in figure 10. The amplitude of the variations in a given section of bend is about twice the one of  $\tau_a$ , the increase in magnitude during the acceleration phase depending on  $x$  and  $z$ . The ratio of the maximum of  $\tau_c$  to the maximum of  $\tau_a$ , decreases during the decelerating phase from about 28% to about 20%. Throughout the pulse cycle, the low shear region (for both  $\tau_a$  and  $\tau_c$ ) appears to be located near the inner wall in the major part of the curved tube, with the flow conditions used in this study.

Values of the axial shear stress in the bend may be compared to these in the upstream straight pipe (Fig. 9). During the end of flow deceleration, as well as during the beginning of flow acceleration, the wall shear is greater or nearly equal, in the bend than in a straight section. It becomes lower than in the straight duct during the end of the accelerating phase and during the beginning of the decelerating phase at the inner wall of the major part of the

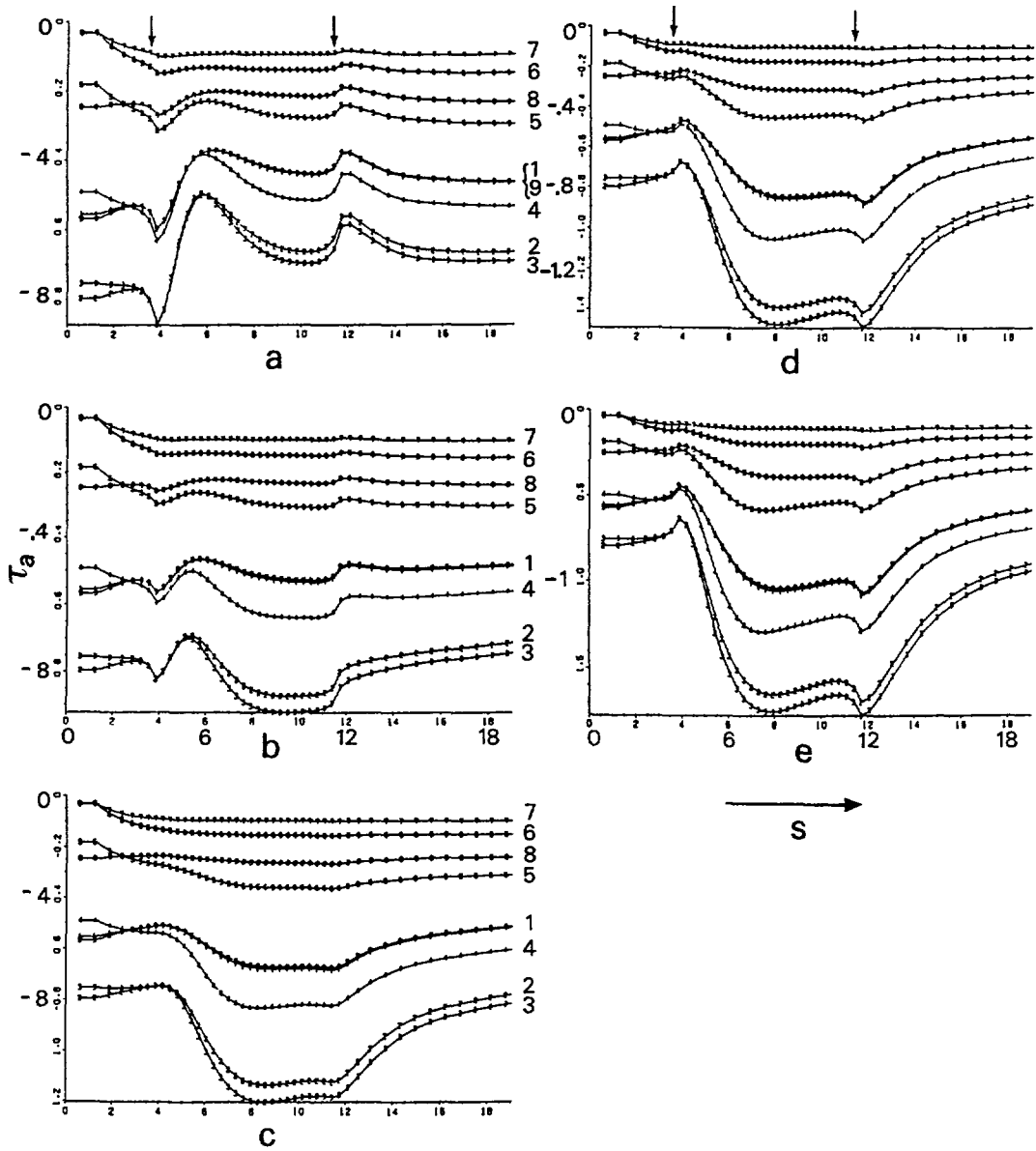


Fig. 9. — Axial shear stress  $\tau_a$  (in  $\text{N}\cdot\text{m}^{-2}$ ) against non-dimensional longitudinal distance ( $s = L/d$  in straight pipe or  $s = Rz/d$  in curved tube) throughout the pulse cycle : ( $t/T = 0$  (1) 0.13 (2) 0.26 (3)  $t = 0.39$  (4) 0.52 (5) 0.61 (6) 0.74 (7) 0.87 (8) 1 (9) at different circumferential angles (from top to bottom, left then right, a :  $18^\circ$  ; b :  $54^\circ$  ; c :  $90^\circ$  ; d :  $126^\circ$  ; e :  $162^\circ$ ). The left and right arrows indicates the locations of the bend inlet and outlet respectively.

bend (Fig. 9a). Its value is also lower in a short segment located in the upstream segment of the bend (whatever  $x$ ) when the instantaneous axial component of the velocity  $W(t)$  is greater than the mean (steady) component  $\bar{W}$ .

The axial velocity profiles in the centerplane, at the beginning of flow deceleration and at

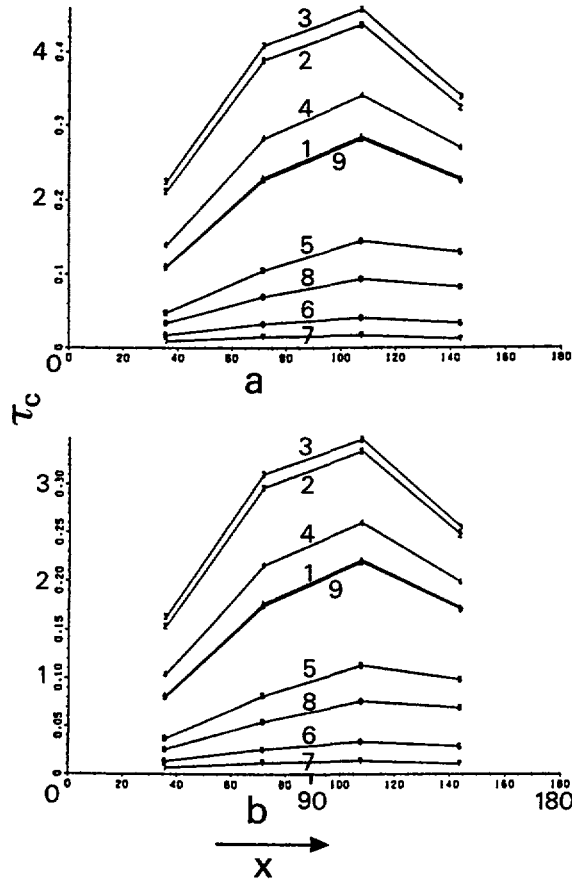


Fig. 10. — Circumferential shear stress  $\tau_c$  (in  $N.m^{-2}$ ) against circumferential angle  $x$  throughout the pulse cycle (same symbols as in Fig. 7) at two selected cross sections in the curved tube (a :  $48.6^\circ$ ; b  $88.2^\circ$ ).

the beginning of flow acceleration, have been superimposed in figure 11. At the beginning of the decelerating phase, the velocity profiles in the downstream part of the curved tube ( $z > 75^\circ$ , i.e. profiles I; J and K) exhibit only slight differences. At  $90^\circ$ , the flow seems to be not far from a fully-developed regime. In contrast, at the beginning of flow acceleration, the profiles can be almost completely superimposed, from a cross section located much nearer the bend inlet ( $z \geq 34^\circ$ ). When the unsteady axial component of the flow is smaller than the mean flow, the curvature affects only slightly the flow ; the secondary motion is very weak and consequently the axial velocity profile is much less distorted. The entry length may then be shorter.

#### 4. Discussion

Inhaled particle deposition (pollutants present in the surrounding medium, radioactive particles, anaesthetic or therapeutic aerosols) depends on the flow characteristics in the airways. Atherogenesis is closely linked to the mass transfer between the blood and the arterial wall.

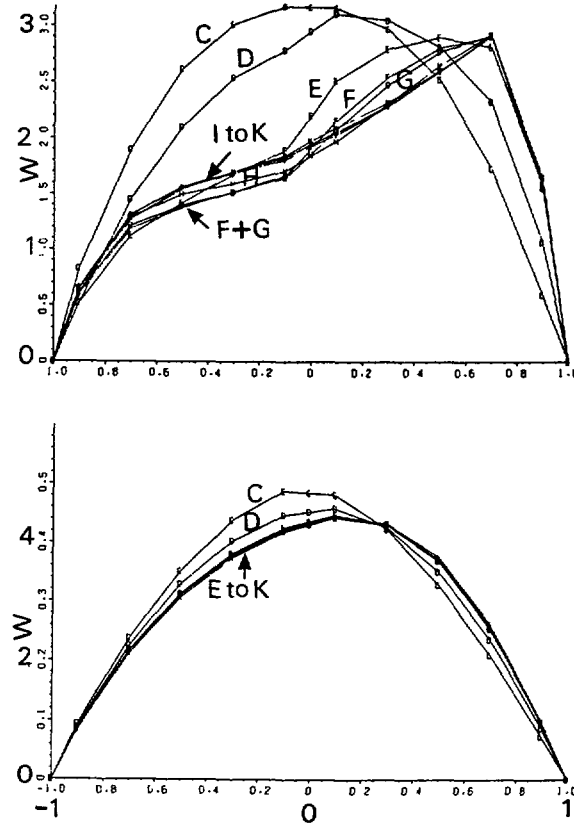


Fig. 11. — Superimposition of axial velocity profiles in the centerplane at different cross sections along the bend (same symbols as in Fig. 6). Top : beginning of flow deceleration. Bottom : beginning of flow acceleration.

The tracheo-bronchial tree, as well as the arterial network, is characterized by numerous sites of branching and curvature. The transport of particles within the vessel lumen and through the vessel wall is quite complex. A reasonable approach is to study the different steps of the mass transfer separately. The present work is focused on the particle deposition of the tube wall which depends on the geometry of the vessel network and the type of flow. Numerical experiments of pulsatile developing flow in a rigid curved tube have therefore been carried out, with a given set of governing parameters, as a preliminary to this work.

The numerical model presents some limitations. The inlet conditions are far from resembling the cardiac output, although a sinusoidal, zero-mean flow would be suitable for airway flow at rest. The pipe wall is rigid, whereas the flow behavior is known to be closely coupled to the mechanics of the compliant wall. The  $90^\circ$  bend of uniform cross-section was not aimed at representing any particular biological curved duct, since such ducts are liable to huge variability along the pipe network, as well as a very large variability of given curved parts of this network among human subjects. As usual, the flow was assumed to be incompressible (with respect to air flow in the respiratory tract) and Newtonian (with respect to blood flow in the central arteries, which are those preferentially affected by atheroma). The main limitation may

arise from the relatively coarse grid used for the computations, although it is not inherent to the numerical model itself but to the computer system used in this work. However, reasonably good agreement has been found, for steady flow, with our experimental results and those furnished by several groups of investigations, despite an overestimation of the shear stress near the inner wall. Such an agreement may be assumed for the present test characterized by a strong steady component. The symmetry condition has been already discussed by Hamakiotes and Berger (1988). This assumption might be irrelevant to flows characterized by a high unsteadiness. At large  $Re_2$ , Lyne (1970) proposed indeed the existence of an additional boundary layer of thickness  $Re_2^{-1/2}$  across the centerplane. Moreover complex secondary motions have been found in unsteady flows for high  $De$  (4, 5, 6), especially in the inner part of the pipe. At the outlet plane of the downstream straight tube, of length  $8.1 d$ , the normal derivatives of the velocity components were assumed to be zero for the exit boundary condition. But this length as an entry for a pulsatile flow appears to be too short in comparison with the length of  $10 d$  generally admitted. However, the fully-developed flow assumption, over a shorter distance, does not seem to introduce any significant reduction in the downstream effect of the curved tube, the secondary motion remaining strong  $2 d$  from the bend outlet.

Variations of axial and circumferential shear stresses during the sinusoidal cycle have been investigated for different sets of governing parameters, at different stations along the curved tube. Unfortunately the values of the flow parameters in the present model do not correspond to those provided by the literature. For similar values of  $\alpha$  and  $De$  ( $\alpha = 4$ ,  $De = 100$ , but  $Re = 1000$ ) Rabadi *et al.* (1980) found that the axial shear stress maximum, located at the outer wall, for a fully-developed flow, is about 4 times lower than in our model with a curvature 10 times larger. The maximum of  $\tau_c$ , moving slightly near the outer part of the upper wall, oscillates also with a lower amplitude during the sinusoidal cycle. Hamakiotes and Berger (1988) studied the pulsatile flow in a bend for much lower ( $Re = 2$ ) or much higher ( $Re = 400$ ) values of the mean Reynolds number. For  $\alpha = 15$ , flow reversal is observed. At  $Re = 400$ , a shift from the outer wall to the inner wall in peak axial shear stress occurs when the axial flow becomes bidirectional. The large changes in  $\tau_a$  magnitude are associated with direction variations. The maximum of  $\tau_c$  remains at the same site (near the vertical diameter slightly toward the outer wall) throughout the cycle. The maximum of  $\tau_c$  is closer to the peak  $\tau_a$  than in our study.

As in test 1 of Chang and Tarbell (1985), no flow reversal is observed. Besides, the computed results as well as flow visualisation experiments have not shown separation in the  $90^\circ$  bend with the fixed geometry and for the given flow regime used in the present work. As soon as separated regions occur, longer residence times within these regions may increase particle deposition and diffusion through the wall.

Atherosclerotic plaques tend to occur in highly reproducible sites. One of the main goals of the study of bend flows will thus be to investigate the role of the flow variables on the cell adhesion on the arterial endothelium and the lipid uptake by the vessel wall. It is now generally admitted that deposits on the tube wall occur in regions of low wall shear. At the beginning of flow deceleration, the wall shear is lower at the inner edge of the major part of the curved tube than in straight pipe. Particle deposits may thus occur at any inner curvature. But at the beginning of flow acceleration, the wall shear is higher in the bend than in the upstream straight section. Consequently, the existence of a curved section may not improve deposition of solid particles during the low flow stage of the cycle. However blood flow, with its typical pressure waveform, is more complex. The governing parameters vary along the vascular bed for a fixed cardiac output. The variations of the wall shear depend thus on the situation along the arterial tree. Moreover, the cardiac output, as well as the vessel geometry, change in response to different stimuli. Consequently, local variations in both magnitude and direction of the

shear stress during the cardiac cycle and its possible range of change during much higher time intervals must be taken into account. Furthermore, the effect of the shear stress depends on the nature and on the time constant of the different particle transfer processes involved in the atherogenesis.

### Acknowledgements.

Financial support of this work was provided by the Royal Society and the Medical Research Council. One of us acknowledges the receipt of grants from Nato, Fondation pour la Recherche Médicale and Association Claude Bernard.

### Appendix

The toroidal dimensional coordinates  $(x, y', z)$  define the most natural system for the curved pipe :  $x$  is the circumferential -,  $y'$  the radial - and  $z$  the streamwise angular coordinate. The origin of the reference system is the center of curvature (Fig. 12). Let  $X, Y, Z$  be the cartesian coordinates of a frame with the same origin, and  $D$  the distance between the projection of a point of any cross-section of the duct in the plane  $Z = 0$ . ( $D = R + y \cos x$ , where  $R$  is the radius of curvature of the centerline).  $X = D \cos z$ ,  $Y = D \sin z$ ,  $Z = y \sin x$ .

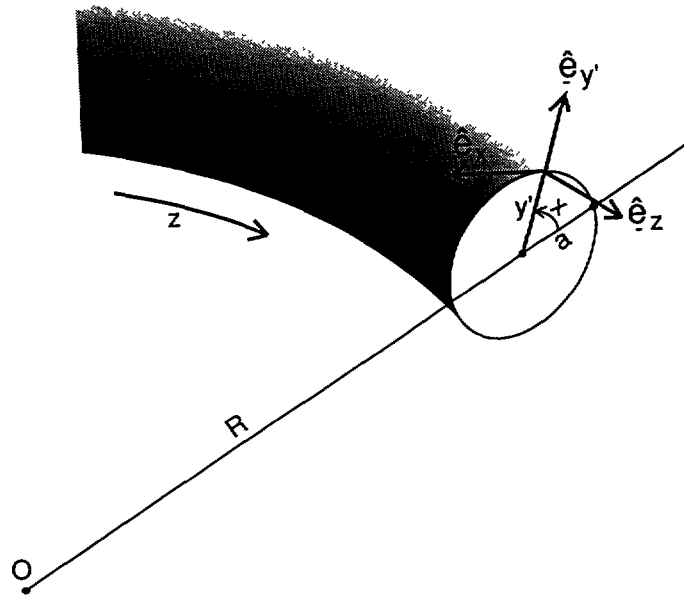


Fig. 12. — Coordinate system in curved pipes ( $a$  is the tube radius,  $R$  the curvature radius of the tube axis),  $\hat{e}$  is a unit vector.

In this suitable orthogonal coordinate system, the continuity equation in its dimensional form becomes :

$$\left(\frac{1}{y'}\right)' + (\cos x/D)u + u_{y'} - (\sin x/D)v + (1/y')v_x - (1/D)w_z = 0,$$

where the subscripts  $x, y', z$  denote partial derivatives.

The three components of the momentum dimensional equation are given respectively by :

$$\begin{aligned}
 1) & \rho (u_t + uu_{y'} + (v/y')(u_x - v) - (w/D)(\cos xw + u_z)) = \\
 & -p_{y'} + \mu \left[ - (1/y'D) (D(v_{y'} + (v/y') - (1/y')u_x))_x + (1/D^2) (u_z + \cos xw + Dw_{y'})_z \right] \\
 2) & \rho (v_t + uv_{y'} + (v/y')(u + v_x) + (w/D)(\sin xw - v_z)) = \\
 & - (1/r)p_x + \mu \left[ (1/D) [(D(v_{y'} + v/y' - (1/y')u_x))_{y'} + ((1/D)(v_z - \sin xw) + (1/r)w_x)_z] \right] \\
 3) & \rho [w_t + uw_{y'} + (v/y')w_x - (w/D)(w_z - \cos xu + \sin xv)] = \\
 & (1/D)p_z + \mu \left[ (1/y) \left[ (y'(w_{y'} + (\cos x/D)w + (1/D)u_z))_{y'} + ((1/y')w_x + (1/D)v_z - (\sin x/D)w_x)_x \right] \right]
 \end{aligned}$$

### References

- [1] LYNE W.H., Unsteady viscous flow in a curved pipe, *J. Fluid Mech.* **45** (1970) 13-31.
- [2] BERTELSEN A.F., An experimental investigation of low Reynolds number secondary streaming effects associated with an oscillating viscous flow in a curved pipe, *J. Fluid Mech.* **70** (1975) 519-527.
- [3] RABADI N.J., SIMON M.A. and CHOW J.C.F., Numerical solution for fully developed, laminar pulsating flow in curved tubes. *Numerical Heat Transfer* **3** (1980) 225-239.
- [4] TALBOT L. and GONG K.O., Pulsatile entrance flow in a curved pipe, *J. Fluid Mech.* **127** (1983) 1-25.
- [5] CHANG L.J. and TARBELL J.M., Numerical simulation of fully developed sinusoidal and pulsatile (physiological) flow in curved tubes, *J. Fluid Mech.* **161** (1985) 175-198.
- [6] HAMAKIOTES C.C. and BERGER S.A., Fully developed pulsatile flow in a curved pipe, *J. Fluid Mech.* **195** (1988) 23-55.
- [7] CARETTO L.S. et al., Two calculation procedures for steady, three-dimensional flows with recirculation, Proc. Third Int. Conf. on numerical methods in fluid dynamics (Paris, 1972) pp. 60-68.
- [8] ISSA R.I., Solution of the implicitly discretised fluid flow equations by operator splitting, Imperial College Report n° FS/82/15, London, 1982.
- [9] STONE H.L., Iterative solution of implicit approximations of multidimensional partial differential equations, *SIAM J. Num. Analysis* **5** (1968) 530-558.
- [10] WOMERSLEY J.R., Method for the calculation of velocity, rate of flow and viscous drag in arteries when the pressure gradient is known, *J. Physiol. London* **127** (1955) 553-563.
- [11] CARO C.G., FITZ-GERALD J.M. and SCHROTER R.C., Arterial wall shear and distribution of early atheroma in man, *Nature* **223** (1969) 1159-1161.
- [12] SNABRE P., BITBOL M. and MILLS P., Cell desaggregation behaviour in shear flow, *Biophys. J.* **51** (1987) 795-807.
- [13] MILLS P. and SNABRE P., Particle migration connected to rheological mechanism in a flowing aggregated suspension. Application to white blood cells margination, *Clinic. Hemorheol.* **7** (1987) 295-304.